Nuclear physics of cosmic ray interaction with semiconductor materials: Particle-induced soft errors from a physicist's perspective

by H. H. K. Tang

The key issues of cosmic-ray-induced soft-error rates, SER (also referred to as single-event upset, SEU, rates) in microelectronic devices are discussed from the viewpoint of fundamental atomic and nuclear interactions between high-energy particles and semiconductors. From sea level to moderate altitudes, the cosmic ray spectrum is dominated by three particle species: nucleons (protons and neutrons), pions, and muons. The characteristic features of high-energy nuclear reactions of these particles with light elements are reviewed. A major cause of soft errors is identified to be the ionization electron–hole pairs induced by the secondary nuclear fragments produced in certain processes. These processes are the inelastic collisions between the cosmic ray particles and nuclei in the host material. A state-of-the-art nuclear spallation reaction model, NUSPA, is developed to simulate these reactions. This model is tested and validated by a large set of nuclear experiments. It is used to generate the crucial database for the soft-error simulators which are currently used throughout IBM for device and circuit analysis. The relative effectiveness

0018-8646/96/$5.00 © 1996 IBM

of nucleons, pions, and muons as soft-error-inducing agents is evaluated on the basis of nuclear reaction rate calculations and energy-deposition analysis.

1. Introduction

It has been known for many years that an ionizing particle passing through an electronic device introduces strong field perturbations. If the intruding particle is near a p-n junction, it may induce a soft error, or single-event upset. The basic physical picture is that excess electron–hole pairs are generated in the wake of the penetrating particle. The field in the neighborhood of the p-n junction, if sufficiently strong, separates these electrons and holes before they recombine, and sweeps the excess carriers of the appropriate sign to a nearby device contact. A random signal is registered if this collected charge exceeds a critical threshold value.

This picture is adequate for the description of soft-error phenomena due to low-energy particles. A well-known example is the alpha particles[1] [1] emitted from radioactive residues which are occasionally present in the packaging materials of integrated circuits [2, 3]. These alphas have kinetic energies typically of the order of several MeV. Some of them are stopped in the device. A key parameter is the stopping power[2], or energy loss per unit track length, which is a measure of the local energy exchange between the incoming particle and the electrons in the medium. It is useful to convert the energy loss into ionization pairs per unit track length. For Si, the conversion factor is 3.6 eV per electron–hole pair [4]. An energy loss of 1 MeV/μm in Si is therefore associated with the generation of 2.8×10^5 electron–hole pairs/μm, which is equivalent to a local linear charge density of ± 44.5 fC/μm. When ionization (ionization pairs/μm) is plotted against particle penetration length, a so-called Bragg curve is obtained. This curve is flat and has small values at small path lengths, but it rises steeply and reaches a maximum value near the end of the particle range. Most of the kinetic energy of the particle is deposited into a narrow Bragg region which surrounds the peak of the ionization curve.

When the intruding particle is a high-energy cosmic ray particle with a kinetic energy of several hundred MeV, the above picture must be modified in a fundamental way. A high-energy particle is very penetrating, and, in general, is not stopped in the device. Since the energy deposited in the host device is small, the excess charge generated by electronic ionization is insufficient to cause soft errors. Nonetheless, soft errors can be induced by other mechanisms of particle interactions. The cosmic ray particles, especially protons, neutrons, and pions, can collide with the nuclei in the semiconductor. The probability of such a collision event is in general very small. However, when a collision occurs, a nuclear reaction is initiated, typically resulting in the emission of secondary nuclear fragments. These fragments consist of pions, protons, neutrons, light ions such as deuterons[3], tritons[4], and helium[5], and heavy residual nuclei[6] such as magnesium, oxygen, and carbon. With the exception of neutrons, all of these reaction products contribute electronic ionization energies. When the total number of ionization electron–hole pairs induced by the secondary fragments produced in a collision exceeds a critical value (which is a characteristic of the device), the memory state of the device can be switched. This microscopic picture was invoked [5] to explain the anomalous malfunctions of spacecraft electronic systems operating in background with strong cosmic ray radiation. The picture is well supported by extensive experimental observations that soft errors are detected when devices and circuits are irradiated by neutrons. (See, for example, References [6–10].) Being electrically neutral, neutrons do not lose energy in the device by electronic ionization. They can only be stopped by neutron–nucleus interactions which, in turn, produce secondary charged fragments.

The charge-collection mechanisms were the focal point of the SER studies reported in Reference [11]. In these studies, the authors used surface barrier detectors as the prototype device and investigated the SER induced by protons.

The work described in this review is motivated by reliability concerns for advanced devices exposed to cosmic ray radiation. The devices are assumed to be operating at sea level to moderate altitudes, that is, altitudes below about 20 km, at which the cosmic ray intensity peaks [9]. Attention is focused on three major cosmic ray components: nucleons (protons and neutrons), pions ($\pi^{\pm}$, π^0), and muons ($\mu^{\pm}$), with kinetic energies from tens of MeV up to 1 GeV. Modeling cosmic-ray-induced

[1] The alpha-particle, ^{4}He, is a stable isotope of helium which consists of two protons and two neutrons.

[2] Niels Bohr was the first to obtain a stopping power formula for a charged particle passing through a medium. The original derivation was based on classical electrodynamics. Subsequent refinements of Bohr's classic work and incorporation of quantum mechanics in the theory were due to H. A. Bethe, F. Bloch, E. Fermi, L. Landau, W. Heitler, J. Ashkin, and many others. The term "linear energy transfer," or LET, is also used in the literature of radiation physics. In most cases, LET (up to a constant of proportionality) is the same as the stopping power, which is energy loss per unit length.

[3] The deuteron, ^{2}H, is an isotope of hydrogen which consists of a proton and a neutron.

[4] The triton, ^{3}H, is an isotope of hydrogen which consists of one proton and two neutrons.

[5] Helium ions in this review mean the isotopes ^{4}He (alpha-particle), or ^{3}He (which consists of two protons and one neutron). In SER-related problems, ^{4}He are far more important than ^{3}He. The production probabilities of ^{4}He from nuclear reactions are at least an order of magnitude larger than those of ^{3}He.

[6] By the current conventions of the high-energy and nuclear physics communities, an isotope with mass number less than 30 is considered to be a light ion. Hence, silicon and all residual nuclei produced from it are light ions. Despite the apparent inconsistency in the term "heavy residual nuclei," it is used throughout the text to highlight the important fact that the ionization energies associated with the residual nuclei are very different from those with the lighter reaction products (protons, deuterons, tritons, and helium).

soft errors consists of two aspects: 1) a microscopic analysis at the level of nuclear particle interactions, and 2) a system analysis at the levels of device and circuit. Ultimately, the modeling capabilities at the device and circuit levels are possible primarily because a general nuclear reaction model, NUSPA[7] [12], has been developed. At the fundamental level of nucleon–nucleus reactions, it has been systematically verified by a large body of nuclear data (see **Table 1**). By means of the NUSPA model, a crucial database is generated for SEMM[8], a simulator for soft-error analysis, which is currently used throughout IBM on a routine basis [2, 3].

This review gives a physicist's scenario of what causes soft errors in microelectronic devices bombarded by high-energy particles. It addresses the key issues of the atomic and nuclear interactions between cosmic ray particles and semiconductors. The arguments and conclusions presented here are based on modern nuclear physics. As such, they are general and are valid for a wide range of technological applications which are of current and future interest. Discussions on soft-error problems in specific devices and systems can be found in the other papers of this special issue [8, 9] or elsewhere [10].

The work on the NUSPA model and its applications in SER analysis was started in 1986. In the initial stage of this development, the primary concern involved applications at sea level, where protons and neutrons play a major role. (See, for example, the cosmic ray spectra shown in Reference [9].) The modeling efforts were accordingly concentrated on proton and neutron reactions. A critical review of nucleon-induced reactions and a status report on comparisons of the NUSPA model with experiments were given in a *Physical Review* paper in 1990 [12]. In recent years, because of growing interest in the reliability issues of devices operating at higher altitudes—environments in which pion intensities are much stronger than at sea level—the NUSPA model was extended to treat pion–nucleus reactions. Currently, studies of pion-induced soft-error phenomena are still in progress. Some new NUSPA results concerning pion–nucleus interactions and their SER implications are presented here for the first time.

In Section 2, the energy loss of charged cosmic ray and secondary particles in silicon is reviewed. In Section 3, nucleon–nucleus interactions are discussed. Their relevance for soft errors in semiconductor devices is emphasized. A brief description is given for the NUSPA model, which is the basic simulation tool for nucleon– and pion–nucleus reactions. In Section 4, pion-induced SERs are discussed in the light of new NUSPA simulations of pion–nucleus reactions. In Section 5, muon–nucleus interactions and their associated SER problems are analyzed. Finally, in Section 6, a summary of the nuclear modeling work is presented.

Table 1 Experimental database used to verify nuclear modeling.

E (MeV)	*Projectiles*	*Targets*	*Measurements*	*Institutions*
27	n	C, N, O	p, d, t, He	UCD
29	p	C, O, Al	p, d, t, He	ORNL
32.2	n	Si	p, d, t, He	UCD
39	p	C, O	p, d, t, He	ORNL
40	n	N, O	p, d, t, He	UCD
50	p	O, Si	He, Li, Be	IUCF
50	p, n	Si	p, d, t, He	UCD
50	$\pi^{\pm}$	C, Al, Si, HI	σ_r, σ_{tot}	TRIUMF
60.7	n	C, N, O	p, d, t, He	UCD
61.7	p	C, O, Al	p, d, t, He	ORNL
65	n	Fe, Sn, Pb	n	UCD
80	p	Si	recoils	UCD–MSU
85	π^{+}	Li, C, Al, HI	π^{+}, σ_{el}, σ_r	PSI
90	p	Al	p, n, d, t, He	MUCF
125	$\pi^{\pm}$	Li, C, Al, HI	$\pi^{\pm}$, σ_{el}, σ_r	PSI
156	p	Al	p, d, t, He	IUCF
165	$\pi^{\pm}$	Li, C, Al, HI	$\pi^{\pm}$, σ_{el}, σ_r	PSI
164	p	Al	p, d, t, He	IUCF
180	p	Al	recoils	IUCF
200	p	C, O, Si	He, Li, Be	IUCF
205	π^{+}	Li, C, Al, HI	π^{+}, σ_{el}, σ_r	PSI
245	π^{+}	Li, C, Al, HI	π^{+}, σ_{el}, σ_r	PSI
315	π^{+}	Li, C, Al, HI	π^{+}, σ_{el}, σ_r	PSI
318	p	C, Al, HI	n	LANL
500	$\pi^{\pm}$	C	$\pi^{\pm}$	LANL
590	p	C, Al, HI	n	LANL
800	p	C, Al, HI	n	LANL

IUCF: Indiana University Cyclotron Facility
LANL: Los Alamos National Laboratory
MSU: National Superconducting Cyclotron Laboratory, Michigan State University
MUCF: Maryland University Cyclotron Facility
ORNL: Oak Ridge National Laboratory
PSI: Paul Scherrer Institute (former Swiss Institute for Nuclear Research)
TRIUMF: Tri-University Meson Facility
UCD: Crocker Nuclear Laboratory, University of California, Davis
HI: heavy ions
σ_{el} elastic cross section
σ_r reaction cross section
σ_{tot} total cross section

2. Energy loss of cosmic ray and secondary particles

In Reference [9], typical spectra of cosmic ray particles are presented. When the charged cosmic ray particles—protons, charged pions ($\pi^{\pm}$), and muons ($\mu^{\pm}$)—pass through a semiconductor device, they exchange energy with the host medium via electromagnetic interactions with the atoms. **Figure 1** shows the stopping power (energy loss per unit length) of these particles in silicon, over a kinetic energy range of 1–1000 MeV. In this energy range, which is relevant for most device applications, the major mechanism of energy loss is electronic ionization in the

[7] NUSPA stands for Nuclear Spallation Reaction Model/Codes. The basic theory, formulated in the framework of a two-step, cascade-statistical approach to nuclear reactions, is discussed in Reference [12]. Similar work related to this approach to nuclear reactions can also be found in the references quoted there. The NUSPA simulation codes were developed by the author. In this review, no distinction is made between the theoretical model and simulation codes.
[8] SEMM stands for Soft-Error Monte Carlo Modeling.

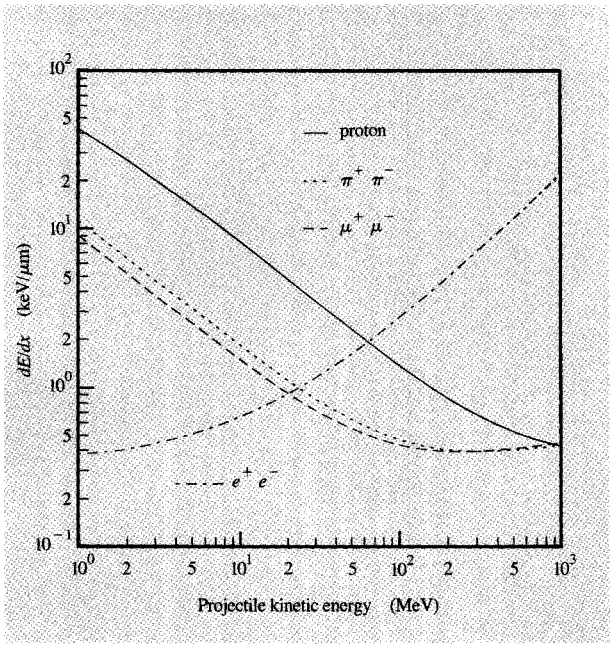

Figure 1

Calculated stopping power of cosmic ray particles (protons, charged pions, muons, electrons, and positrons) in ^{28}Si.

semiconductor medium. The energy loss of proton, pion, and muon, denoted in Figure 1 by the solid, dotted, and dashed curves, respectively, is computed from a standard Bethe–Bloch-type theory[9] [13–15]. Below 1 GeV these three curves are qualitatively similar, except that the stopping power of a proton is several times larger than that of a pion or muon with the same kinetic energy. Electrons and positrons[10] are present in the cosmic rays as the stable decay products of muons. Their stopping power is computed from a Bethe stopping power equation and a Bethe–Heitler equation [16] and is shown in Figure 1 by the dot-dashed curve. For electrons and positrons, the energy loss is dominated by bremsstrahlung effects[11]. This is the main reason why the electron (positron) curve rises rapidly with increasing kinetic energy. For protons, pions, and muons, energy loss due to bremsstrahlung is negligible below 1 GeV.

For a charged cosmic particle passing through a thin Si sample, the energy deposited in the host material is obtained from a linear approximation,

$$\Delta E \simeq \frac{dE}{dx} \Delta x. \tag{1}$$

In (1), dE/dx is the stopping power. For a particle with a kinetic energy of several hundred MeV passing through 50 μm of silicon, ΔE is of the order of 50 keV. The stopping power increases considerably at lower energies. For many applications at sea level, however, low-energy charged cosmic ray particles (say, below 50 MeV) are not expected to give serious SER problems. This is because very few of these particles can penetrate the shielding atmosphere.

For each incoming cosmic ray particle (whether it be charged or uncharged), there is a small but finite probability of collision with an atomic nucleus in the host medium. There are two classes of nuclear collisions: elastic and inelastic scattering. In most elastic events, the cosmic ray particle is deflected slightly from its original trajectory (small-angle scattering) and deposits a small amount of energy onto the target nucleus, which recoils but does not change its intrinsic energy state. Large-angle scatterings are very unlikely. In contrast, large energies are exchanged in inelastic events. In the initial stage of an inelastic event, secondary protons, neutrons, and pions are produced, and an excited intermediate nucleus is formed. This nucleus subsequently de-excites by the emission of other secondary particles, and it is finally transformed into a stable and lighter residual nucleus. These particle-generating processes take place at the expense of the binding energy of the parent nucleus. The secondary fragments from the second reaction stage consist of protons, neutrons, light ions such as deuteron, triton, and helium, and heavy residual nuclei. The energy spectrum of the secondary protons is wide. The kinetic energy of such protons can be close to the incident energy of the cosmic ray particles, or it can be as low as 1 MeV or less. Low-energy protons deposit appreciable ionization energies (per unit track length) in the host material. The light ions have mean kinetic energies of a few MeV, and they are associated with large ionization energies. **Figure 2** shows the stopping power curves of helium, triton, and deuteron in silicon. For a given projectile energy, the stopping power of any of these light ions is greater than the proton stopping power. The final residual nucleus produced in an inelastic collision typically has a kinetic energy of a few MeV. Because of its small velocity, its range is shorter and its stopping power is greater than that of the lighter ions.

[9] The stopping power curves of proton, pion, and muon in Figure 1 are obtained from a standard Bethe–Bloch-type theory, formulated in the framework of a second-order Born approximation. The mean excitation potential of Si is taken to be 174.5 eV. For the muon calculations, corrections due to spin-1/2 particle scattering have been neglected. The total stopping power of electron and positron is a sum of electronic ionization and radiation energy loss due to bremsstrahlung. The electronic ionization part is computed by a Bethe equation, and the bremsstrahlung part is computed by a Bethe–Heitler equation.

[10] A positron (e^+) is an anti-particle of the electron (e^-). Its properties are identical to those of the electron (i.e., same mass, spin, and charge), except that the charge it carries is positive. In modern particle physics, electrons, positrons, muons, and their associated neutrinos are members of a class of elementary particles called leptons, which are believed to be point-like.

[11] Bremsstrahlung is the energy loss due to radiation suffered by a charged particle which moves with a large velocity in the strong electromagnetic field of a nuclear target. It is different from electronic ionization and is a major process of energy loss for light particles such as electrons and positrons. For heavier charged particles such as muons, pions, and protons, bremsstrahlung effects are usually negligible, except when the particles are at ultra-relativistic velocities.

The secondary particles—the light charged ions and heavy residual nuclei—because of their higher charges and smaller kinetic energies, deposit larger ionization energies in the semiconductor medium than do the incoming cosmic ray particles. Unlike the high-energy cosmic ray particles, their ranges are short. Some of the secondary fragments cannot escape from the region in which they are produced; hence, their kinetic energies are dissipated over a small volume in the host medium. High-energy nucleon–nucleus or pion–nucleus collisions often produce high multiplicities of secondary charged fragments, and the total energy deposited from such an event is in the MeV range. The event creates in Si a large number of spurious electron–hole pairs, which in turn are very effective in inducing soft errors if they are generated near a p-n junction in an operating device. The fundamental problem to resolve is twofold. First, for each kind of cosmic ray particle, what is the frequency with which the inelastic nuclear collisions occur? Second, once the nuclear collisions have taken place, what are the characteristic energy and angular distributions of the secondary fragments? To address these crucial questions, the interactions between the cosmic ray particles and nuclei must be critically examined.

3. Nucleon–nucleus interaction

Interactions between a nucleon (proton or neutron) and a nucleus can be either an elastic or an inelastic scattering event. In an elastic scattering event, symbolically represented by

$$\text{nucleon} + \text{target} \rightarrow \text{nucleon} + \text{target}, \tag{2}$$

the nucleon does not excite the target nucleus. This process is analyzed by standard proton- and neutron–nucleus optical models [17–19]. In the subsection on elastic nucleon–nucleus scattering, it is shown that elastic nucleon–nucleus collisions involve small recoil energies; hence, they play a relatively minor role in soft-error failures in most device applications. (However, elastic collisions are important in radiation problems of thick media where multiple scatterings must be considered.)

The inelastic nucleon–nucleus scatterings include all nucleon-induced reactions of the type

$$\text{nucleon} + \text{target} \rightarrow X_1 + X_2 + \cdots + X_n + \text{residual nucleus}. \tag{3}$$

In (3), the reaction products $X_1, X_2, \cdots, X_n$ can be proton, neutron, deuteron, triton, and helium. When the kinetic energy of the incident nucleon exceeds 280 MeV, secondary pions can also be produced. In an inelastic collision event, the identity of the incoming projectile is lost, and the creation of secondary particles is associated with energy exchanges which are of the order of MeV or larger. Since these inelastic collisions are considerably more complex than elastic scatterings, special reaction models must be developed for their analysis.

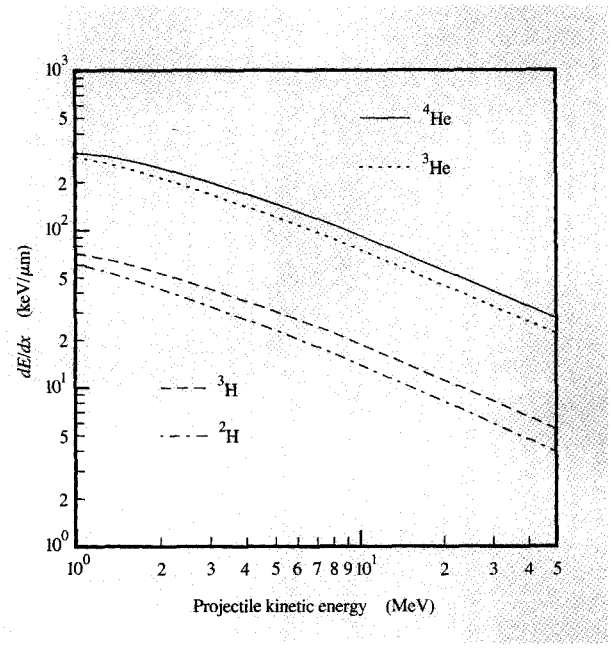

Figure 2

Calculated stopping power of secondary light ions (helium, triton, and deuteron) in ^{28}Si.

Consider a Si sample with thickness Δx, irradiated by nucleons. This thickness represents the depth of the active region in a device. Unless stated otherwise in the following discussions, it is always assumed to be small ($\Delta x < 50$ μm). The probability that a cosmic ray particle will pass through the sample without any nuclear collision (elastic or inelastic) is given by the transmission formula

$$P_T = \exp(-\rho \sigma_{tot} \Delta x). \tag{4}$$

In (4), ρ is the number of Si atoms per unit volume (cm^{-3}), and σ_{tot} is the total nucleon–nucleus scattering cross section, which is usually given in units of millibarns (1 mb = 1×10^{-27} cm^2). The total nucleon–nucleus cross section consists of two parts,

$$\sigma_{tot} = \sigma_r + \sigma_{el}, \tag{5}$$

where σ_r and σ_{el} are the (inelastic) reaction cross section and the elastic cross section, respectively. In **Figure 3**, the reaction and total cross sections of neutrons on ^{28}Si are plotted against neutron energy. The reaction cross section (solid curve) is computed from the NUSPA model, which is discussed in the following sections. For the total cross section (dotted curve), the elastic cross-section component

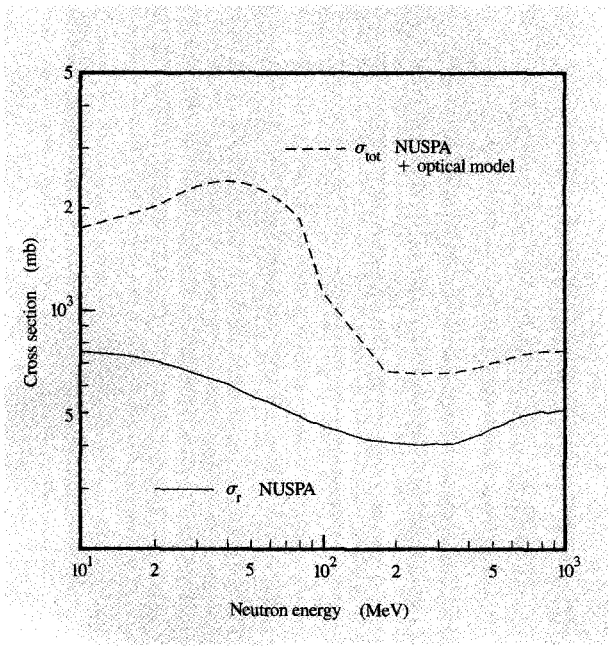

Figure 3

Calculated reaction and total cross sections of neutrons on ^{28}Si as functions of neutron energy. The inelastic reaction cross section, denoted by the solid curve, is computed from the NUSPA model. The total cross section, denoted by the dashed curve, is the sum of the elastic and (inelastic) reaction cross sections. The elastic cross section is obtained from optical model calculations.

(shape elastic) is constructed from optical model calculations [20]. It is significant to note that the nucleon–nucleus cross sections are energy-dependent, and they are large at low energies. Also, the energies of the cosmic ray nucleons span a wide range from tens of MeV up to GeV [9]. If these features—energy dependence of the nuclear cross sections and cosmic ray flux—are taken into account, the reaction or collision rate (number of nuclear collisions per unit time) due to elastic and inelastic events in a Si sample is given by

$$R_{NC} = A \int_{E_{min}}^{E_{max}} dE\phi(E)\{1 - \exp[-\rho\sigma_{tot}(E)\Delta x]\}. \quad (6)$$

In (6), $\phi(E)$ is the energy flux of the cosmic ray nucleons expressed in units of particle number-cm^{-2}-s^{-1}-MeV^{-1}; E_{min} and E_{max} are the lower and upper energy limits of the cosmic ray spectrum; A is the surface area of the sample exposed to the cosmic rays. For simplicity, the cosmic ray flux is assumed to be normal to the surface of the sample, though any angular dependence of the flux can be included in the analysis in a straightforward manner. For a thin sample (<50 μm), the condition $\rho\sigma_{tot}(E)\Delta x \ll 1$ is always satisfied, and the reaction rate (6) can be reduced to a simpler formula,

$$R_{NC} \simeq \rho A\Delta x \int_{E_{min}}^{E_{max}} dE\phi(E)\sigma_{tot}(E). \quad (6a)$$

The meaning of (6a) is apparent: $\phi(E)\sigma_{tot}(E)dE$ is the reaction rate per nuclear target (Si) due to the cosmic ray nucleons in the energy interval $[E, E + dE]$, and $\rho A\Delta x$ is the number of scattering centers in the sample. If a typical high-energy nucleon–Si total cross section of 600 mb is used (see Figure 3), for a Si sample 20 μm thick, the probability of an incoming particle encountering a nuclear collision in the sample is estimated to be $\rho\sigma_{tot}\Delta x \simeq 6 \times 10^{-5}$. For a monoenergetic unit flux (1 particle-cm^{-2}-s^{-1}) irradiating a sample with surface area of 50 μm × 50 μm and a depth of 20 μm, the reaction rate is estimated to be $R_{NC} \simeq 1.5 \times 10^{-9}$ s^{-1}.

The reaction rate R_{NC} corresponding to a radiation background gives a rough estimate for the probability of soft-error fails. However, not every nuclear collision leads to a soft error. For a given collision event, several key factors determine the outcome: the distribution of the ionization energies of the secondary particles, the location of the collision site, and also the operating conditions of the device in question. Hence, in order to carry out rigorous and complete soft-error analyses, the distributions of the secondary nuclear fragments and device structure must enter the simulations.

- *Elastic nucleon–nucleus scattering*

As an example, **Figure 4(a)** shows the elastic angular distribution of 100-MeV protons scattered off the ^{28}Si target, obtained from optical model calculations [20]. For a Si sample with surface area A, depth Δx, and number density ρ (atoms per unit volume), irradiated by a monoenergetic proton beam (100 MeV in this case) with flux I_0 (protons per unit area per unit time), the number of protons elastically scattered into a certain solid angle in unit time is given by

$$\Delta N_{el} = \rho A\Delta x I_0 \frac{d\sigma}{d\Omega}\Delta\Omega$$

$$= \rho A\Delta x I_0 \frac{d\sigma}{d\Omega}\sin\theta\Delta\theta\Delta\phi. \quad (7)$$

In (7), $\Omega(\theta, \phi)$ denotes the polar coordinates, and the direction of the incident protons is used to define the polar axis; $\Delta\Omega = \sin\theta\Delta\theta\Delta\phi$.

As is typical of such reactions, the angular distribution is forward-peaked. More than 90% of the protons are scattered into a forward cone subtended by a polar angle of 20°. The probability of a proton being scattered into large angles is very small. There is a one-to-one correspondence between the projectile scattering angle and the kinetic energy of the recoil target nucleus. In **Figure 4(b)**, the recoil energy of the ^{28}Si nucleus is plotted against the

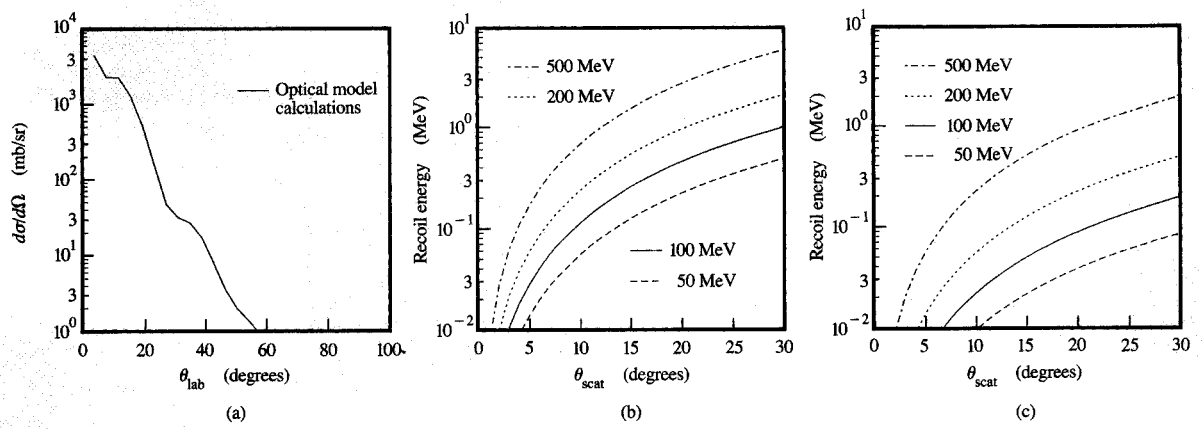

Figure 4

(a) Angular distribution of elastic scattering of 100-MeV protons off ^{28}Si, obtained from optical model calculations. The angular distribution is plotted against the scattering angle measured in the laboratory system. (b) Kinetic energy of recoil nucleus as function of proton scattering angle, for elastic scatterings of 50-, 100-, 200-, and 500-MeV protons off ^{28}Si. (c) Kinetic energy of recoil nucleus as function of pion scattering angle, for elastic scatterings of 50-, 100-, 200-, and 500-MeV pions off ^{28}Si.

proton scattering angle, for proton incident energies of 50, 100, 200, and 500 MeV. At scattering angles less than 30°, except for very high incident energies, the recoil energy is only a fraction of 1 MeV. Compared with the energy exchanged in a typical inelastic collision, the elastic recoil energy is small. Similar conclusions can be reached for elastic pion–nucleus collisions. Examples of high-energy pion–nucleus scattering can be found in References [21] and [22]. **Figure 4(c)** shows the recoil energy of the ^{28}Si nucleus plotted against the pion scattering angle for pion energies of 50, 100, 200, and 500 MeV. At angles less than 30°, the recoil energy is small.

At low energies (tens of MeV), the total elastic proton- and neutron–nucleus cross sections are large and are of the order of barns[12] (see Figure 3). In low-energy reactions, elastic collisions can be as frequent as, or even more frequent than, inelastic collisions. A fundamental SER issue comes up. Can elastic collision events alone cause soft errors in a device? For example, in a device which requires a critical charge (Q_{crit}) of 50 fC to flip its memory, it would take a minimum ionization energy of 1.12 MeV to induce such a switch. Figure 4(b) shows that a recoil energy with this magnitude is not possible except from large-angle scatterings—events which are very unlikely. (In elastic scatterings of protons or neutrons, the maximum recoil energy for the ^{28}Si nucleus is reached in a backward-scattering event. In this special case, the recoil energy is $0.133E$, where E is the nucleon incident energy in MeV.) Hence, for devices with Q_{crit} larger than 50 fC, elastic collisions in general are very inefficient in inducing soft errors. However, for future devices with Q_{crit} smaller than 50 fC, the elastic collisions may not be negligible when the devices are exposed to low-energy protons and neutrons.

From now on, the discussion is focused on the inelastic collisions only. The probability for a nucleon to encounter inelastic collisions in a thin Si sample of thickness Δx is given by

$$P_C = 1 - \exp(-\rho\sigma_r\Delta x). \tag{8}$$

In Appendix A, a formal proof is given to show that Equation (8) is consistent with basic transport theory, Equations (4) and (5), and the observation that the elastic cross sections are forward-peaked. Analogous to (6), the reaction rate associated with inelastic nucleon–nucleus collisions in a sample is given by

$$R'_{NC} = A\int_{E_{min}}^{E_{max}} dE\phi(E)\{1 - \exp[-\rho\sigma_r(E)\Delta x]\}$$

$$\simeq \rho A\Delta x\int_{E_{min}}^{E_{max}} dE\phi(E)\sigma_r(E). \tag{9}$$

The second line of (9) is due to the assumption of a thin sample.

- *Inelastic nucleon–nucleus scattering*

For accurate modeling of soft errors at the device and circuit level, knowledge of the distributions of secondary

[12] The barn is a unit of cross section commonly used in high-energy and nuclear physics; 1 barn = 1×10^{-24} cm^2. In nuclear processes, 1 barn is considered to be a "large" cross section.

fragments from the inelastic nucleon–nucleus collisions is essential. It is not enough that one can compute the nucleon–nucleus reaction cross sections at all projectile energies; one must also be able to predict the production rates of various secondary reaction products as functions of energy and angle. These crucial physical quantities are deduced from cross sections which are computed or measured. Combined with stopping-power calculations, these production rates allow one to compute the ionization energies generated in an inelastic event. An exact treatment of this problem would require a global analysis of all exclusive reaction channels[13] of the nucleon–nucleus system. For collisions in the hundred-MeV range, typically hundreds of reaction channels are opened up. A full quantum treatment of the multi-channel reaction dynamics from first principles is neither practical nor possible. Phenomenological models are often used for practical applications.

A nuclear spallation reaction model is developed in the framework of a two-step cascade-statistical approach. On the basis of this model, a system of Monte Carlo simulation codes, generically called NUSPA codes, has been developed. Two crucial concepts are invoked: intranuclear-cascade-type processes and compound nuclear reactions. The ideas of intranuclear cascades were originally formulated for high-energy reactions by Serber in 1947 [23], and were developed by Goldberger in the 40's [24], by N. Metropolis et al. in the 50's [25], and by Bertini [26] and others[14] in the 60's and 70's. The notion of compound nucleus formation was introduced by Bohr in 1937 [27], and was based on Bohr's so-called Independence Hypothesis. Models of compound nucleus reactions were subsequently developed by Weisskopf [28, 29] and others in the 40's and 50's. A critical discussion on modern versions of the cascade-statistical approach to nucleon–nucleus reactions and applications of NUSPA for light elements are given in Reference [12]. The main features of the model are now summarized.

The nucleon–nucleus reaction is assumed to take place in two stages which involve different time scales. In the first stage (intranuclear cascade process), the incident proton or neutron interacts with the target nucleus via a sequence of two-body, quasi-free scatterings between the projectile and target nucleons. This process results in secondary protons, neutrons, and pions, most of which are emitted in the forward direction from the parent nucleus. The reaction time for the cascade process is of the order of 10^{-21}–10^{-22} s. The model inputs are free nucleon–nucleon and pion–nucleon cross sections which are known from experiments with good precision. The simulations are based on Monte Carlo methods. Since the adopted statistical sampling techniques incorporate (approximately) the Fermi momenta of the target nucleons and the Pauli exclusion principle, many of the important medium correction effects for the nucleon–nucleus system are included [12]. At the end of the first stage, an excited compound nucleus [27–30] is formed.

In the second stage, the statistical decay of the excited compound nucleus is associated with many complex intermediate processes and a longer reaction time which is of the order of 10^{-16}–10^{-19} s. Protons, neutrons, and light ions such as deuterons, tritons, and helium are emitted randomly and isotropically in the rest frame of the compound nucleus. The emission probabilities of these decay channels are determined by the excitation energy, the level density of the compound nucleus, and the inverse capture cross sections of the emitted particles. The calculations of these quantities are discussed in Reference [12].

This model has several features which are unique and useful for soft-error applications. First, the model generates absolute cross sections. That is, the model simulations do not require arbitrary normalizations with respect to any prior measurements; consequently, the calculations can be directly tested by nuclear experiments. Second, all exclusive reaction channels of the final states compatible with energy-momentum conservation are simulated on an equal footing, even though in practice a relatively small number of one-particle inclusive spectra[15] are sufficient for most applications. On the practical side, the computational methods adopted (Monte Carlo samplings and simulations on an event-by-event basis) provide a convenient means of generating the crucial database for the soft-error simulator, SEMM. A subtle, but more important, advantage of the model is that a certain class of fundamental sum rules[16] [31, 32] is automatically satisfied. These sum rules set up rigorous constraints on the reaction cross section and the cross sections of all reaction channels. Since the model gives good predictions of the reaction cross section as well as the dominant channels (proton, neutron, and light ions), the sum rule

[13] In a nucleon–nucleus reaction, nucleon + target $\rightarrow X_1 + \cdots + X_n$ + residual nucleus, if the energies and momenta of all fragments $X_1, \cdots, X_n$ and the residual nucleus are measured, the measurement is said to be exclusive. The cross section obtained is called an exclusive cross section. A given combination of secondary fragments is called a reaction (exit) channel. The set of exclusive cross sections of all possible exit channels constitutes the complete information on the reaction. A similar terminology applies to pion–nucleus reactions.

[14] Some of the most popular intranuclear cascade codes which have been used by various national laboratories and research groups for basic and applied research include the MECC code of Bertini [12, 26], the HECT code, which is a high-energy transport code developed from the MECC code, and the VEGA code [K. Chen, Z. Fraenkel, G. Friedlander, J. R. Grover, J. M. Miller, and Y. Shimamoto, *Phys. Rev.* **166**, 949 (1968)].

[15] In a nucleon–nucleus reaction, the symbol *nucleon + target* $\rightarrow F + X$ is used to denote an experiment in which the energy and momentum of a particular secondary fragment F (pion, nucleon, light ion, or residual nucleus) is measured, irrespective of the energies and momenta of any other fragments X released in the same event. This measurement is said to be inclusive, and the cross section obtained is called a one-particle inclusive cross section. Starting from the complete set of all exclusive cross sections of a nucleon–nucleus system, a particular inclusive cross section can be derived. However, in general, the knowledge of all inclusive cross sections alone is insufficient to reconstruct the exclusive channels.

[16] The author is indebted to J. L. Romero, who pointed out the usefulness of exploiting the sum rules.

feature guarantees that the model also gives a good description of the distributions of recoil nuclei, which are a major source of ionization energy.

Over the energy range 20 MeV–1 GeV, the NUSPA model systematically predicts the nucleon–nucleus reaction cross sections to within 5–10% of the experimental data. An example is shown in **Figure 5**, in which the theoretical reaction cross sections of a proton on ^{28}Si, ^{16}O, and ^{12}C are compared with the compiled data of Reference [33]. Hence, the collisional probability of a cosmic ray proton or neutron at a given incident energy and for a given semiconductor sample can be accurately predicted. This in turn implies that the basic reaction rate given in Equations (6), (6a), (8), and (9) can be reliably calculated once the cosmic ray flux is known.

The model is shown to reproduce a large body of nuclear data. In particular, there is a consistent agreement between theory and experiments for the inclusive spectra of the dominant channels—protons, neutrons, helium, and residual nuclei. Details of this comparison are given in Reference [12]. Table 1 is a summary of the database against which the model is stringently tested; it is an extension of the original database of Reference [12]. A few of the neutron experiments [34–37] and all of the pion experiments listed in Table 1 have been added after 1990. As emphasized in Reference [12], in testing the model, the simulations are done with one set of input model parameters, and they are directly compared with the existing data without *ad hoc* adjustments. Furthermore, it should be emphasized that this reaction model provides a scheme in which all dominant channels (protons, neutrons, light ions, and heavy residual nuclei) are simulated within the same theoretical framework. This is particularly significant for soft-error analysis, since all charged secondary fragments (which deposit ionization energies in the semiconductor medium) are treated by one kinematically self-consistent model.

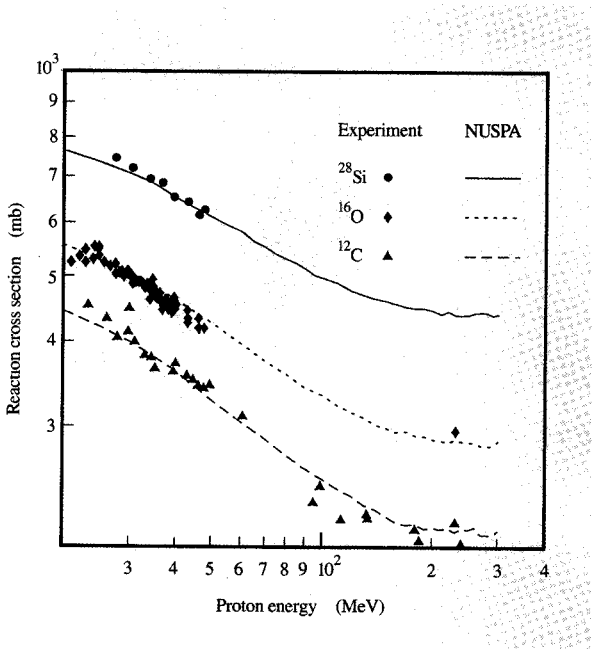

Figure 5

Reaction cross sections of proton on three light isotopes. The solid, dotted, and dashed curves are computed from the NUSPA model for ^{28}Si, ^{16}O, and ^{12}C, respectively. The circles, diamonds, and triangles represent experimental data compiled in Reference [33].

• *Numerical example*

In order to demonstrate the basic points in the above discussion, some details are now worked out for a particular exit channel from the reaction of 200-MeV neutrons on ^{28}Si. At this energy, a large number of exit channels are energetically possible. The following is an example taken from the Monte Carlo outputs of a NUSPA simulation. In the first stage of the reaction (cascade process),

$$n + {}^{28}\mathrm{Si} \rightarrow 2p + 2n + {}^{25}\mathrm{Mg}^{*}. \qquad (10a)$$

After two protons and two neutrons have been emitted from the system, an excited compound nucleus ^{25}Mg* is formed. It then de-excites by particle emission (statistical decay, or evaporation),

Table 2 Example of a high-energy reaction channel for 200-MeV n + ^{28}Si.

Secondary particle	*K. E.* (MeV)	*dE/dx* (keV/μm)	*e-h pairs/μm*	*Range* (μm)
p	5.224	13.51	3.75×10^3	225
p	4.195	15.91	4.43×10^3	155
n	65.478	0	0	∞
n	22.958	0	0	∞
n	6.815	0	0	∞
^{4}He	12.218	79.91	2.22×10^4	90.5
^{4}He	12.025	80.83	2.25×10^4	88.1
^{4}He	7.881	108.84	3.02×10^4	43.6
^{12}C	4.138	1253.34	3.48×10^5	3

$$^{25}\mathrm{Mg}^{*} \rightarrow n + 3\,^{4}\mathrm{He} + {}^{12}\mathrm{C}. \qquad (10b)$$

In process (10b), a neutron and three alpha-particles are emitted from the compound nucleus ^{25}Mg*, which is transformed into a residual nucleus ^{12}C. **Table 2** displays the kinematic details of the secondary fragments. The kinetic energies, stopping powers, ionization rates (ionization electron–hole pairs per unit length), and maximum ranges of the fragments are shown. Note that

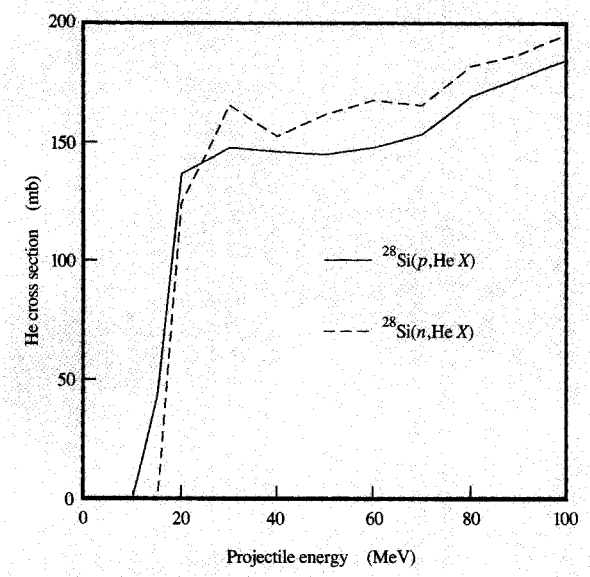

Figure 6

Comparison of helium (^{3}He + ^{4}He) production cross sections from the reactions p + ^{28}Si and n + ^{28}Si. The solid and dashed curves represent He (integrated) cross sections from the proton and neutron reactions, respectively, plotted against projectile kinetic energy.

the ionization rate is largest for the ^{12}C residual nucleus, followed by the alpha-particles. A secondary proton with 4 or 5 MeV gives an ionization rate that is small compared with that of a typical alpha-particle. It may appear that the major contribution to ionization comes from the residual nucleus. However, in high-energy reactions, the frequency of events with alpha multiplicity greater than 1 is high. In these events, as the present example shows, the combined ionization rates of several alphas in an event can be comparable to the ionization rate from one recoil nucleus. Also, in the high- as well as low-energy reactions, the cross sections from the slow secondary protons (with kinetic energies below a few MeV) are in general not small. They constitute a source of ionization which is not negligible in many applications. Some of these observations have been discussed in the context of a simple but realistic energy-deposition model for silicon slabs irradiated by protons [38].

- *Protons versus neutrons*

The proton and neutron can be regarded as different isotopic spin states of the same nuclear system. The isotopic symmetry is exact if the strong (nuclear) interaction is the only force in operation. In reality this symmetry is broken by the electromagnetic interaction, which is manifested in the slightly different rest masses of proton and neutron. The characteristics of high-energy proton–nucleus and neutron–nucleus reactions are very similar (above 100 MeV). This situation is exploited in the SER work. From field measurements, the cosmic ray neutron flux at sea level is found to be much larger than proton flux [9]. Until recently, high-energy neutron (accelerator) experiments have not been readily available, so the proton–neutron similarity has been exploited, and high-energy proton experiments have been used to verify the simulation models at both the nuclear and device levels.

At low energies, because of the Coulomb interaction, the proton and neutron can no longer be treated as the same particle. **Figure 6** shows the NUSPA calculations of the He (^{3}He + ^{4}He) production cross sections from the p + ^{28}Si reaction (solid curve), and the n + ^{28}Si reaction (dashed curve), at projectile energies below 100 MeV. For a Si sample irradiated by protons or neutrons (with energy E), the He production rate (number of ions per unit time) from inelastic collisions is given by

$$\Delta N_{\mathrm{He}} = \rho A \Delta x I_0 \sigma_{\mathrm{He}}(E). \qquad (11)$$

In (11), ρ, A, and Δx are the sample parameters specified in the subsection on elastic nucleon–nucleus scattering; I_0 is the nucleon flux (particles per unit area per unit time); $\sigma_{\mathrm{He}}(E)$ is the He cross section at nucleon energy E.

The He cross sections from the neutron reactions are somewhat larger than those from the proton reactions. At low energies, because the number of accessible reaction channels is small, the qualitative features of these spectra are easily understood from the viewpoint of reaction Q-values. For example, in the alpha-producing channel of the proton reaction,

$$p + {}^{28}\mathrm{Si} \rightarrow {}^{4}\mathrm{He} + {}^{25}\mathrm{Al} \qquad Q = -7.714\ \mathrm{MeV}, \qquad (12)$$

whereas in the alpha-producing channel of the neutron reaction,

$$n + {}^{28}\mathrm{Si} \rightarrow {}^{4}\mathrm{He} + {}^{25}\mathrm{Mg} \qquad Q = -2.654\ \mathrm{MeV}. \qquad (13)$$

A minimum energy of 7.714 MeV must be supplied to initiate reaction (12), and 2.654 MeV for reaction (13). Because of the lower Q-value, the alpha-producing channel of (13) is energetically more favorable than that of (12). This is consistent with the NUSPA result shown in Figure 6 and can be viewed as a consequence of Coulomb interactions. The residual nucleus ^{25}Al has one more proton than ^{25}Mg. The effect of the extra Coulomb repulsion is manifested by the fact that the nuclear binding energy of ^{25}Al is 5.060 MeV lower than that of ^{25}Mg. This is directly reflected in the Q-values of reactions (12) and (13).

Neutrons are slightly more effective in inducing soft errors than protons at particle energies below 100 MeV

and for the same proton and neutron fluxes. This is because $(n,^4\text{He}\ X)$ cross sections are somewhat larger than the corresponding $(p,^4\text{He}\ X)$ cross sections[17], while the isotopic distributions of the residual nuclei from the protons and neutrons are very similar. From about 20 MeV or below, the proton reaction cross section decreases rapidly because of the proton–nucleus Coulomb barrier. This barrier, however, does not apply to neutrons. In the 10-MeV range, the neutron–nucleus cross sections are large, and the (n, α) cross sections do not vanish. For devices exposed to low-energy neutrons, one may expect some residual soft-error failures below 20 MeV.

4. Pion–nucleus interactions

The cascade-statistical approach is shown to be successful in constructing the distributions of the secondary fragments from nucleon–nucleus reactions [12]. A similar methodology can be used for pion–nucleus reactions. In the NUSPA code, a pion option is developed for this class of reactions. However, a few cautionary remarks are in order.

The cascade-statistical approach to nucleon–nucleus reactions can be shown to be a limiting case of a more general formalism due to Feshbach, Kerman, and Koonin (FKK) [39]. The FKK approach is based on nuclear many-body theory, and it has been accepted as part of the tenets of modern nuclear reaction theory [19, 30, 40]. However, rigorous connections between the semiclassical cascade-statistical method and a fundamental field-theoretic framework of pion–nucleus reactions have not yet been established.

There are at least three difficulties for a cascade-statistical model for pion–nucleus reactions. First, the cascade-statistical approach assumes a classical picture of the incident particle. With a rest mass of about 0.14 nucleon mass, the intrinsic wave-mechanical nature of a pion is much more pronounced than that of a nucleon with the same kinetic energy. Furthermore, it is well known that the pion mean free path in a nuclear medium is long and is of the order of several fermis (1 fm = 10^{-12} cm) for reactions at several hundred MeV. (The radius of a ^{28}Si nucleus is about 3.6 fm.) Second, the formation and propagation of quasi-bound pion–nucleon states (Δ resonance) in the nuclear interior are important. The propagation of these states is not properly incorporated in the present model, and the effects of such states on the spectra of the secondary fragments are not well understood. Third, systematic measurements such as $(\pi^{\pm},p\ X)$, $(\pi^{\pm},n\ X)$, and $(\pi^{\pm}$, light ions), against which reaction models can be rigorously tested, are lacking.

[17] It should be pointed out that, below 20 MeV, the concept of an intranuclear cascade is questionable, and the NUSPA model must be modified for very low-energy reactions. That the proton and neutron curves in Figure 6 cross near 20 MeV should be treated as an artifact of the model.

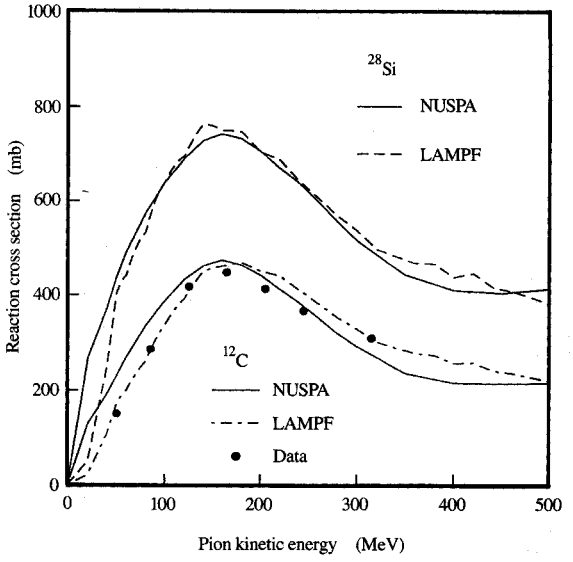

Figure 7

Reaction cross sections of π^+ on ^{28}Si and ^{12}C. The solid curves are theoretical results from the NUSPA model. The dashed and dot-dashed curves are computed from a LAMPF parametrization prescribed in References [41] and [42]. The circles represent data from References [43] and [44].

Despite these theoretical uncertainties, it is seen below that some overall features of inelastic pion–nucleon collisions are reasonably well reproduced by the present version of NUSPA. The implications of these simulations for soft errors are to be assessed.

As with the proton and neutron reactions, it is of primary importance to check that the overall pion-induced reaction rates are correctly predicted. **Figure 7** shows the reaction cross sections of π^+ on ^{28}Si and ^{12}C. The solid curves are the theoretical results from NUSPA calculations. The dashed and dot-dashed curves are obtained from a LAMPF parametrization [41, 42] derived to fit a recent compilation of pion–nucleus cross-section measurements. This parametrization serves to extrapolate to systems or energy regions for which data are not available. The circles represent data taken from References [43] and [44]. For pion kinetic energies up to at least 500 MeV, the theoretical results agree systematically with the data and LAMPF parametrizations to within 10–15%, except at very low energies. Below 100 MeV, the model tends to overestimate the reaction cross section. **Table 3** shows NUSPA calculations of pion–nucleus reaction cross sections for heavier systems, compared with some older data. Agreement between theory and experiments is better

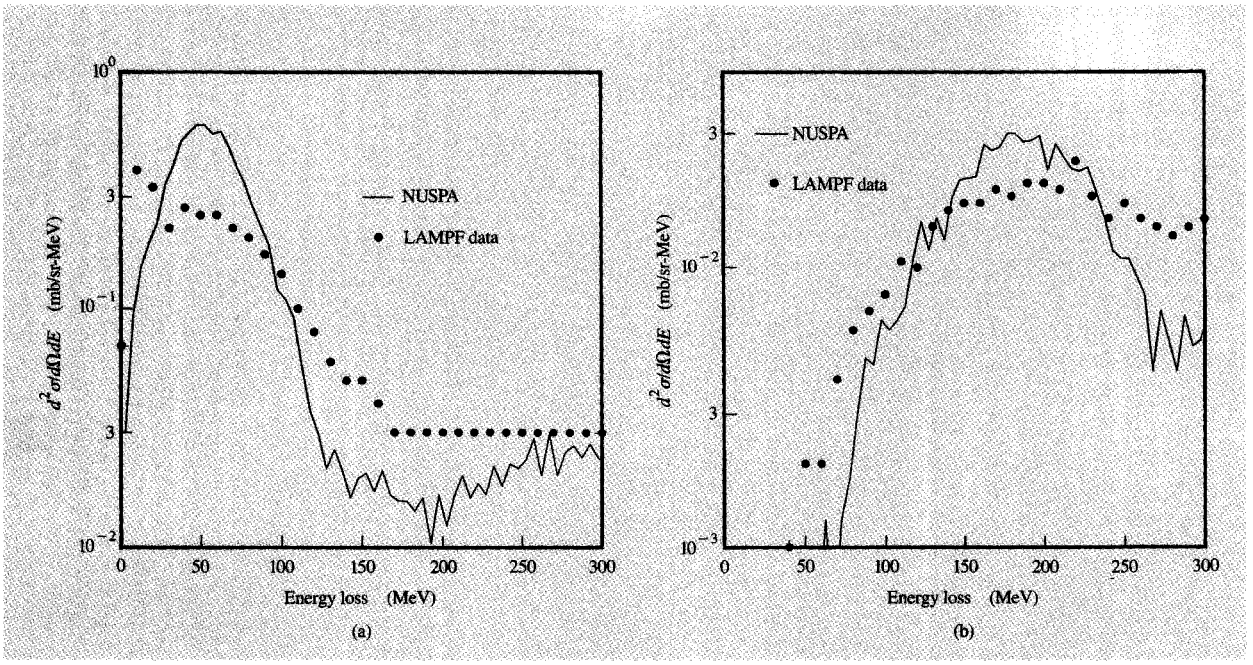

Figure 8

Double differential inclusive spectra of secondary pions at (a) 30° and (b) 70°, from the reaction 500 MeV $\pi^+ + {}^{12}C$. The π^+ spectra are measured in the laboratory system and are plotted against energy loss of the secondary pions. The solid curves are theoretical results from the NUSPA model. The circles represent data taken at the P. Anderson Meson Physics Facility of the Los Alamos National Laboratory [45, 46].

Table 3 Pion–nucleus reaction cross sections—a comparison of NUSPA calculations with experiments.

Pion–nucleus system	*Pion energy* (MeV)	*Reaction cross section* (mb)	
		NUSPA	*Experimental*
$\pi^- + {}^{27}Al$	225	620	600 ± 30
$\pi^- + {}^{64}Cu$	225	1038	1058 ± 45
$\pi^- + {}^{119}Sn$	225	1471	1550 ± 70
$\pi^+ + {}^{208}Pb$	50	1563	1620 ± 50
$\pi^- + {}^{208}Pb$	125	2062	2477 ± 385
$\pi^- + {}^{208}Pb$	150	2145	2490 ± 160
$\pi^- + {}^{208}Pb$	225	2000	2290 ± 90

than 20%. Hence, the theoretical predictions of pion–nucleus reaction cross sections appear to be quite reasonable, and reliable calculations of reaction rates (9) can be done.

Figure 8 shows examples of double differential inclusive spectra[18] of secondary pions (π^+) from the reaction of 500-MeV π^+ on ^{12}C. The spectra at laboratory angles of 30° and 70° are shown. The cross sections are plotted against pion energy loss (kinetic energy of incident pion − kinetic energy of outgoing pion). The solid curves are calculated from the NUSPA model; the circles represent recent data taken at the Los Alamos National Laboratory [45, 46]. The model reproduces the overall features of the experimental spectra at all angles.

The results of reaction cross sections and pion-inclusive spectra indicate that the NUSPA model has incorporated some essential physics of pion–nucleus dynamics. However, these are by no means definitive tests for the model. Pion–nucleus reactions are still an active field of basic nuclear research. It should be pointed out that the present experimental database of pion–nucleus reactions is still incomplete for extensive SER applications. More theoretical and experimental work focused on the charged-fragment exit channels of pion–nucleus reactions and studies of the dominant excitation modes in pion–nucleus systems remains to be done in the near future.

Both the pions and the nucleons interact strongly with the nucleus. It is important to compare nucleon–nucleus and pion–nucleus reactions. A key question with respect to SER phenomena is how the nuclear target is excited by the incident pion or nucleon. The dominant excitation modes

[18] For a thin Si sample bombarded by π^+, the double differential inclusive cross section gives the production rate of secondary π^+, in the energy range of $(E-\Delta E/2, E+\Delta E/2)$ and measured in a solid angle $\Delta\Omega$, that is,

$\rho A \Delta x I_0 (d^2\sigma/d\Omega dE)$,

where I_0 is the incident π^+ flux in units of particle number-cm^{-2}-s^{-1}; ρ, A, and Δx have the same meaning as the parameters of (7).

directly affect the distributions of the secondary fragments which deposit ionization energies in the host material. **Figure 9** shows the energy spectra of secondary He and the excitation spectra of recoil nuclei (in the cascade step) from the reactions $p + {}^{28}\text{Si}$ and $\pi^+ + {}^{28}\text{Si}$, at projectile energies of 250, 500, and 750 MeV. The spectra are simulated by the NUSPA model. The solid and dashed curves denote the results from the pion and proton reactions, respectively. The excitation spectra are constructed as follows. The cascade processes are simulated on an event-by-event basis. At the end of each cascade event, the excitation energy of the recoil nucleus is computed (total energy of recoil nucleus − rest mass of the recoil nucleus at ground state − kinetic energy). These excitation energies of the simulated events are collected to construct a histogram which is normalized with respect to the reaction cross section. For an incident flux I_0 of protons or pions (particles per unit area per unit time), irradiating a Si sample, the number of recoil nuclei produced per unit time, associated with excitation energies in an interval $[E - \Delta E/2, E + \Delta E/2]$, is given by

$$\Delta N_{ex} = \rho A \Delta x I_0 \Delta E \times \{\text{excitation spectrum at energy } E\}. \quad (14)$$

At energies of about 200–400 MeV, it is significant to note that the He cross sections from the pion reactions are much larger than the He cross sections from the proton reactions. Also, the excitation spectra of the recoil nuclei are higher for the pion case. This is consistent with the fact that the coupling between the pion and the nucleon is very strong in this energy region, which shows up in the pion–nucleus reaction cross section (Figure 7). This implies that over this energy region the pions are more effective in exciting the nuclear target than the nucleons, and subsequently secondary fragments are produced at higher rates in pion reactions. This also means that in this energy range, for the same incident flux of cosmic ray particles, the pions are more effective in causing soft errors than protons. At energies above 500 MeV, however, the He spectra and recoil excitation spectra are similar for the pion and proton cases.

For devices operating at sea level, where the pion intensity is more than one order of magnitude lower than the neutron intensity [9], the cosmic-ray-induced soft errors are primarily due to the nucleons. Here contributions of pion-induced SER can be regarded as a higher-order correction to the total SER. At higher altitudes, however, due to the higher pion intensities, their effects are more pronounced than at sea level, and these cosmic ray pions should be treated explicitly in SER analysis.

The above discussion of pion–nucleus interactions applies to energetic pions. Authors of References [47] and [48] suggest another class of processes with which pions induce soft errors. When negative pions are stopped by the materials surrounding the device, they can be captured by the nuclei. The rest mass of the π^- (139.5669 MeV/c^2) is absorbed by the nuclear target, which then de-excites by the emission of secondary fragments. Microscopically [49], this process is thought to proceed by the capture of π^- by a nucleon pair (proton–neutron or proton–proton). The nucleons are ejected into the vacuum, or they can initiate intranuclear cascades which lead to the emission of secondary particles. The energy distributions of cosmic ray pions are in general not well determined. Except under the controlled conditions of accelerator experiments (Reference [47] and work quoted therein), it is difficult in realistic situations to make quantitative estimates of SER contributions due to the stopped pions. It is likely that these capture processes play some significant role in applications at high altitudes, where pion fluxes are larger than at sea level.

5. Muon problem

Unlike protons, neutrons, and pions, the interaction of cosmic ray muons with the nuclei in the semiconductor material does not involve strong nuclear forces. In many respects, a muon behaves like a heavy electron ($m_\mu = 105.659$ MeV/c^2, $m_e = 0.51100$ MeV/c^2), except that it is unstable, with the following dominant decay mode [50] (mean life = 2.197×10^{-6} s):

$$\mu^+ \rightarrow e^+ + \bar{\nu}_\mu + \nu_e, \quad (15a)$$

$$\mu^- \rightarrow e^- + \nu_\mu + \bar{\nu}_e. \quad (15b)$$

In (15a) and (15b), ν_μ and ν_e are the neutrinos associated with the muon and the electron, respectively. The bars above ν denote anti-particles.

Below 1 GeV, the muon stopping power is very close to that of a charged pion (see Figure 1). Hence, a typical high-energy muon, with a kinetic energy of hundreds of MeV, deposits only a small ionization energy as it passes through a thin Si sample. This energy alone would be insufficient to cause soft errors.

As a positive muon slows down in the host medium, it can capture an electron to form a muonic atom, which is unstable. The μ^+ decays into a positron, and the muonic atom is transformed into an e^+e^- system, whose destiny would be pair annihilation due to collisions with other electrons:

$$e^+ + e^- \rightarrow 2\gamma. \quad (16)$$

This sequence of processes involves energies of the order of MeV. (The e^+e^- annihilation process alone releases an energy of 1.022 MeV.) For the above processes to take place, the μ^+ must be slowed down so that its kinetic energy is in the keV range and the muon can capture an orbital electron from a host atom. Since a high-energy

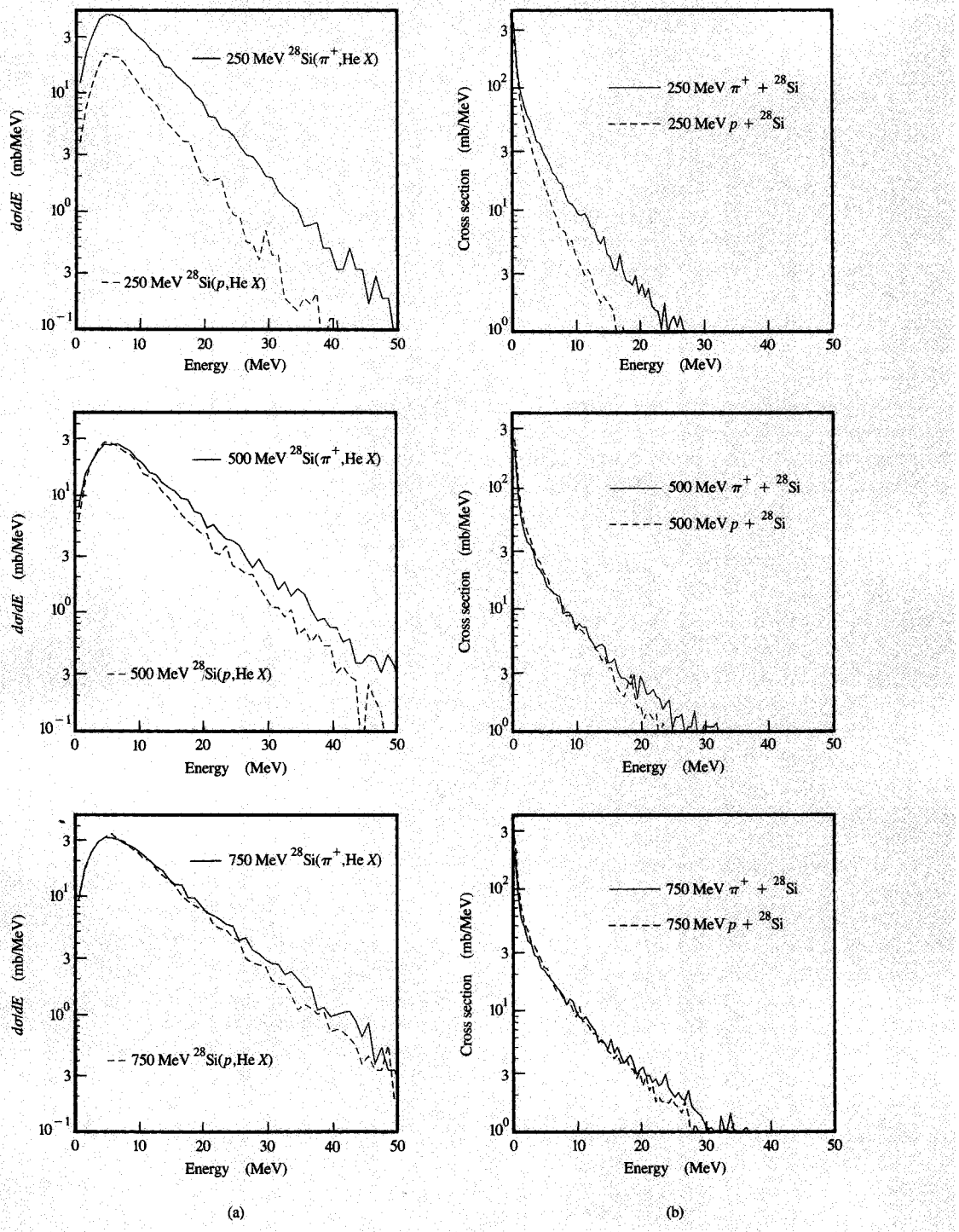

Figure 9

Comparison of (a) secondary He energy spectra and (b) excitation spectra of recoil nuclei from the reactions $\pi^+ + {}^{28}\mathrm{Si}$ and $p + {}^{28}\mathrm{Si}$, at projectile kinetic energies of 250, 500, and 750 MeV. The spectra are computed from the NUSPA model. The solid and dashed curves denote the results for the pion and proton reactions, respectively.

muon has a long range and cannot be slowed down significantly in the thin Si sample for the above processes to occur, these processes need not be considered in the soft-error analysis (unless there are significant sources of slow muons).

As a negative muon slows down in the host medium, it can fall into an orbit of an atom by knocking off its electron (via Coulomb scattering). It then cascades into lower orbits until it reaches the 1s orbit. The Bohr radius of the 1s muon is about 1/207 of that of an electron, and the spatial overlap of the muon wavefunction with the nuclear charge distribution is non-negligible. In about a microsecond, the muon falls into the nucleus and is captured by a target proton via the weak process:

$$\mu^- + p \rightarrow n + \nu_\mu \,. \tag{17}$$

The residual nucleus (with one proton less) can be in an excited state, and de-excites by gamma ray, or light particle, emission. However, for this muon capture to be possible, the incoming μ^- must be slowed down to the keV range. For high-energy muons, the probability of causing soft errors in devices by this capture process is negligible.

6. Summary and conclusion

Cosmic-ray-induced soft-error rates are analyzed by focusing on three major components of the high-energy cosmic ray particles: nucleons (protons and neutrons), pions, and muons. The salient features of the atomic and nuclear interactions between the cosmic ray particles and the semiconductor materials are reviewed. On the basis of general energy-deposition arguments, soft errors are shown to be due primarily to the secondary reaction fragments produced in the inelastic nucleon– and pion–nucleus collisions in the host medium. Under appropriate conditions, these secondary particles generate a sufficiently large number of ionization electron–hole pairs in the neighborhood of a p-n junction to cause a change in the memory state of a device.

A state-of-the-art nuclear spallation model, NUSPA, has been developed. It has been stringently tested by a large body of nuclear data from nucleon–nucleus and pion–nucleus reactions over a wide energy range (tens of MeV to 1 GeV). The model is used to generate the crucial database required by the soft-error simulator, SEMM, which has been extensively used throughout IBM in the past few years.

In the early years of the SER project, the main concern was device applications at sea level, where neutrons and protons constitute the major part of the cosmic ray. Attention was focused on nucleon-induced SERs. The NUSPA model played a critical role in the simulations of inelastic nucleon–nucleus collisions. In applications at higher altitudes, pion effects are expected to be non-negligible. So far, the NUSPA simulations are able to reproduce the overall features of some pion–nucleus reactions. However, because of the strong pion–nucleon coupling over the energy region of 100–300 MeV, more theoretical and experimental work in this energy region is needed in the future. In addition, the SER induced by stopped pions should also be examined. This will make the SER analysis more complete.

Acknowledgments

Many colleagues, inside and outside IBM, deserve thanks for their assistance and involvement in various aspects of the SER project. A few names affiliated with IBM should be specially mentioned. The author was first introduced to the SER work by N. Azziz, who was a collaborator in an initial stage of the project. P. C. Murley and R. R. O'Brien diligently shouldered the burden of the SEMM code numerics, and in addition had to suffer the physicist's temperament of the author. J. L. Walsh and G. R. Srinivasan are to be thanked for their managerial support. The author is indebted to colleagues at several nuclear research institutions: Argonne National Laboratory, Brookhaven National Laboratory, Crocker Nuclear Physics Laboratory of the University of California at Davis, Indiana University Cyclotron Facility, Livermore National Laboratory, Los Alamos National Laboratory, National Superconducting Cyclotron Laboratory at the Michigan State University, and Oak Ridge National Laboratory. Their generous advice on nuclear reactions and radiation physics has been most valuable at all stages of the project. H. W. Bertini's pioneering work on intranuclear cascade models provided a very general theoretical framework from which the present work was started.

Appendix A

A formal proof is now given for Equation (8), which gives the probability of inelastic nuclear collision events in a sample. Consider nucleon transport in a Si slab with a thickness L. Let the number density of scattering centers (number of atoms per unit volume) be ρ. The beam direction is taken to be along the x-axis. For an incoming nucleon, there are two mutually exclusive possibilities: a) propagation through the target from $x = 0$ to $x = L$, without any nuclear collisions, and b) propagation from $x = 0$ to $x = L$, encountering at least one nuclear collision. A nuclear collision is either an elastic or an inelastic event.

The probability for an incoming nucleon to propagate over an interval $[0, x]$ without any nuclear collision is

$$P_T(x) = \exp(-\rho\sigma_{tot}x). \tag{A1}$$

In (A1), σ_{tot} is the total cross section,

$$\sigma_{tot} = \sigma_r + \sigma_{el}\,, \tag{A1a}$$

where σ_r and σ_{el} are the (inelastic) reaction cross section and elastic cross section, respectively. Since the target is assumed to be thin, the small energy loss of the nucleon due to stopping power in the target is ignored, and thus the energy dependence of σ_r, σ_{el}, and σ_{tot} is suppressed. It is convenient to introduce a collisional probability density $P_C(x)$, such that $P_C(x)\delta x$ is the probability that a nucleon will encounter at least one nuclear collision in the interval $[x, x + \delta x]$. It is straightforward to show that

$$P_C(x) = \rho\sigma_{tot} \exp(-\rho\sigma_{tot}x). \tag{A2}$$

As has been pointed out in the text, elastic nucleon–nucleus scatterings are characterized by forward-peaked angular distributions. In a typical elastic collision event, the incoming nucleon is only slightly deflected by the much heavier target nucleus, and suffers very little loss of its kinetic energy. The identity of an elastically scattered nucleon is not lost in the collision event, in contrast to an inelastic collision event, in which the identity of the incident nucleon is lost and the nucleon is removed from the beam. From now on, large-angle scatterings are completely ignored. The transmitted and elastically scattered nucleons are regrouped into a new class. The objective is to compute the probability for all events in this class.

For a nucleon to reach point x, the following cases are considered. The nucleon can reach point x without encountering any collision (case of no collision). The nucleon can encounter one elastic collision at some intermediate point x_1 $(0 < x_1 < x)$ before reaching point x (case with one elastic collision). The nucleon can encounter two elastic collisions at some intermediate points x_1, x_2 $(0 < x_1 < x_2 < x)$ before reaching point x (case with two elastic collisions). In general, the nucleon can encounter N elastic collisions at points $x_1, x_2, \cdots, x_N$ $(0 < x_1 < x_2 < \cdots < x_N < x)$ before reaching x (case of N elastic collisions). The probability for the case of transport with N elastic collisions, $P_N(x)$, must be computed.

In the simplest case of transport without collision, the probability is

$$P_0(x) = P_T(x) = \exp(-\rho\sigma_{tot}x). \tag{A3}$$

In the general case of N elastic collisions, the probability for a nucleon to propagate over $[0, x_1]$ and then encounter an elastic collision in the interval $(x_1, x_1 + \delta x_1)$ is given by

$$\rho\sigma_{tot} \exp(-\rho\sigma_{tot}x_1)\left(\frac{\sigma_{el}}{\sigma_{tot}}\right)\delta x_1\,.$$

The probability for the nucleon to propagate over $[x_1, x_2]$ and encounter an elastic collision in the interval $[x_2, x_2 + \delta x_2]$ is given by

$$\rho\sigma_{tot} \exp[-\rho\sigma_{tot}(x_2 - x_1)]\left(\frac{\sigma_{el}}{\sigma_{tot}}\right)\delta x_2\,.$$

The probability for a nucleon to encounter elastic collisions in the intervals $[x_1, x_1 + \delta x_1]$, $[x_2, x_2 + \delta x_2], \cdots, [x_N, x_N + \delta x_N]$ is given by the joint probability

$$\begin{aligned}
&\rho\sigma_{tot} \exp(-\rho\sigma_{tot}x_1)\left(\frac{\sigma_{el}}{\sigma_{tot}}\right)\rho\sigma_{tot} \\
&\quad\cdot \exp[-\rho\sigma_{tot}(x_2 - x_1)]\left(\frac{\sigma_{el}}{\sigma_{tot}}\right)\cdots\rho\sigma_{tot} \\
&\quad\cdot \exp[-\rho\sigma_{tot}(x_N - x_{N-1})]\left(\frac{\sigma_{el}}{\sigma_{tot}}\right) \\
&\quad\cdot \exp[-\rho\sigma_{tot}(x - x_N)]\delta x_1\delta x_2\cdots\delta x_N \\
&= (\rho\sigma_{el})^N \exp(-\rho\sigma_{tot}x)\delta x_1\delta x_2\cdots\delta x_N\,.
\end{aligned}$$

The probability for having N elastic collisions over $[0, x]$ is given by

$$\begin{aligned}
P_N(x) &= \int_0^x dx_1 \int_{x_1}^x dx_2 \cdots \int_{x_{N-1}}^x dx_N(\rho\sigma_{el})^N \exp(-\rho\sigma_{tot}x) \\
&= \frac{(\rho\sigma_{el}x)^N}{N!}\exp(-\rho\sigma_{tot}x).
\end{aligned} \tag{A4}$$

The total probability of transport over $[0, x]$ with transmission and elastic collisions is given by the sum of these partial probabilities P_N,

$$\begin{aligned}
P'_T(x) &= \sum_{N=0}^{N=\infty} P_N(x) \\
&= \exp(-\rho\sigma_{tot}x) + \frac{\rho\sigma_{el}x}{1!}\exp(-\rho\sigma_{tot}x) \\
&\quad + \frac{(\rho\sigma_{el}x)^2}{2!}\exp(-\rho\sigma_{tot}x) + \cdots \\
&\quad + \frac{(\rho\sigma_{el}x)^N}{N!}\exp(-\rho\sigma_{tot}x) + \cdots \\
&= \exp(-\rho\sigma_{tot}x)\left[1 + \frac{\rho\sigma_{el}x}{1!} + \cdots + \frac{(\rho\sigma_{el}x)^N}{N!} + \cdots\right] \\
&= \exp(-\rho\sigma_{tot}x)\exp(\rho\sigma_{el}x) \\
&= \exp[-\rho(\sigma_{tot} - \sigma_{el})x] \\
&= \exp(-\rho\sigma_r x).
\end{aligned} \tag{A5}$$

In arriving at the last result, Equation (A1a) has been used; hence, the probability for the class of transmission and elastic events combined is just the transmission probability using the reaction cross section alone. The probability of inelastic collision is

$$P_C(x) = 1 - P'_T(x) = 1 - \exp(-\rho\sigma_r x), \quad \text{(A6)}$$

which is the result of Equation (8) in the text.

References

1. C. M. Hsieh, P. C. Murley, and R. R. O'Brien, "A Field-Funneling Effect on the Collection of Alpha-Particle-Generated Carriers in Silicon Devices," *IEEE Electron Device Lett.* **EDL-2**, 103–105 (1981).
2. G. R. Srinivasan, "Modeling the Cosmic-Ray-Induced Soft-Error Rate in Integrated Circuits—An Overview," *IBM J. Res. Develop.* **40**, 77–89 (1996, this issue).
3. P. C. Murley, "Soft-Error Monte Carlo Modeling Program, SEMM," *IBM J. Res. Develop.* **40**, 109–118 (1996, this issue).
4. K. G. McKay and K. B. McAfee, "Electron Multiplication in Silicon and Germanium," *Phys. Rev.* **91**, 1079–1084 (1953).
5. P. J. McNulty, "Charged Particles Cause Microelectronics Malfunction in Space," *Phys. Today* **36**, 9 (1983).
6. C. S. Guenzer, E. A. Wolicki, and R. G. Allas, "Single Event Upset of Dynamic DRAMs by Neutrons and Protons," *IEEE Trans. Nucl. Sci.* **NS-26**, 5048–5052 (1979).
7. E. Normand, W. J. Stapor, P. McNulty, W. G. Abdel-Kader, and M. H. Yaktieen, "Quantitative Comparison of Single Event Upsets Induced by Protons and Neutrons," *IEEE Trans. Nucl. Sci.* **38**, 1457–1462 (1991).
8. J. F. Ziegler, H. W. Curtis, H. P. Muhlfeld, C. J. Montrose, B. Chin, M. Nicewicz, C. A. Russell, W. Y. Wang, L. B. Freeman, P. Hosier, L. E. LaFave, J. L. Walsh, J. M. Orro, G. J. Unger, J. M. Ross, T. J. O'Gorman, B. Messina, T. D. Sullivan, A. J. Sykes, H. Yourke, T. A. Enger, V. Tolat, T. S. Scott, A. H. Taber, R. J. Sussman, W. A. Klein, and C. W. Wahaus, "IBM Experiments in Soft Fails in Computer Electronics (1978–1994)," *IBM J. Res. Develop.* **40**, 3–18 (1996, this issue).
9. J. F. Ziegler, "Terrestrial Cosmic Rays," *IBM J. Res. Develop.* **40**, 19–39 (1996, this issue).
10. *Ionizing Radiation Effects in MOS Devices and Circuits*, T. P. Ma and P. V. Dressendorfer, Eds., John Wiley & Sons, Inc., New York, 1989.
11. P. J. McNulty, "Energy Deposition in Microstructures in Si and GaAs," *Report No. DNA-TR-89-225*, U.S. Defense Agency, Alexandria, VA, March 1991.
12. H. H. K. Tang, G. R. Srinivasan, and N. Azziz, "Cascade Statistical Model for Nucleon-Induced Reactions on Light Nuclei in the Energy Range 50 MeV–1 GeV," *Phys. Rev. C* **42**, 1598–1622 (1990).
13. B. T. Price, "Ionization by Relativistic Particles," *Rep. Prog. Phys.* **XVIII**, 52–82 (1955).
14. S. V. Starodubtsev and A. M. Romanov, "The Passage of Charged Particles Through Matter," trans. from Russian, Israel Program for Scientific Translations, Jerusalem, 1965.
15. J. F. Janni, "Proton Range-Energy Tables, 1 keV–10 GeV," *Atom. Data & Nucl. Data Tables* **27**, 147–339, 341–529 (1982).
16. W. Heitler, *Quantum Theory of Radiation*, 3rd Ed., Clarendon Press, Oxford, 1954.
17. A. Bohr and B. Mottleson, *Nuclear Structure, Vol. I: Single-Particle Motion*, Addison-Wesley Publishing Co., Inc., Reading, MA, 1992.
18. A. DeShalit and H. Feshbach, *Theoretical Nuclear Physics, Volume 1: Nuclear Structure*, John Wiley & Sons, Inc., New York, 1974.
19. G. R. Satchler, *Nuclear Direct Reactions*, Oxford University Press, New York, 1982.
20. E. H. Auerbach, *Report No. BNL 6562* (ABACUS optical model code), Brookhaven National Laboratory, Brookhaven, L.I., NY, 1982.
21. C. M. Chen, D. J. Ernst, and M. B. Johnson, "High-Energy Pion–Nucleus Elastic Scattering," *Phys. Rev. C* **48**, 841–849 (1993).
22. M. W. Rawool-Sullivan, C. L. Morris, J. M. O'Donnell, R. M. Whitton, B. K. Park, G. R. Burleson, D. L. Watson, J. Johnson, A. L. Williams, D. A. Smith, D. J. Ernst, and C. M. Chen, "Pion Elastic Scattering on ^{28}Si at T_π = 400 MeV," *Phys. Rev. C* **49**, 627–629 (1994).
23. R. Serber, "Nuclear Reactions at High Energies," *Phys. Rev.* **72**, 1114–1115 (1947).
24. M. L. Goldberger, "The Interactions of High Energy Neutrons and Nuclei," *Phys. Rev.* **74**, 1269–1277 (1948).
25. N. Metropolis, R. Bivins, M. Storm, A. Turkovich, J. M. Miller, and G. Friedlander, "Monte Carlo Calculations on Intranuclear Cascades. I. Low-Energy Studies," *Phys. Rev.* **110**, 185–203 (1958).
26. H. W. Bertini, "Intranuclear-Cascade Calculation of the Secondary Neutron Spectra from Nucleon–Nucleus Interactions in the Energy Range 340 to 2900 MeV and Comparisons with Experiments," *Phys. Rev.* **188**, 1711–1730 (1969).
27. N. Bohr, *Nature* **137**, 344 (1936).
28. V. Weisskopf, "Statistics and Nuclear Reactions," *Phys. Rev.* **52**, 295–303 (1937).
29. J. M. Blatt and V. F. Weisskopf, *Theoretical Nuclear Physics*, John Wiley & Sons, Inc., New York, 1952.
30. P. E. Hodgson, "Compound Nucleus Reactions," *Rep. Prog. Phys.* **50**, 1171–1228 (1987).
31. C. E. DeTar, D. Z. Freedman, and G. Veneziano, "Sum Rules for Inclusive Cross Sections," *Phys. Rev. D* **4**, 906–909 (1971).
32. D. Horn and F. Zachariasen, *Hadron Physics at Very High Energies*, Frontiers in Physics Series, W. A. Benjamin, Inc., 1973.
33. W. Bauhoff, "Tables of Reaction and Total Cross Sections for Proton–Nucleus Scatterings Below 1 GeV," *Atom. Data & Nucl. Data Tables* **35**, 429–447 (1986).
34. E. L. Hjort, "Elastic and Inelastic Neutron Scattering at 65 MeV," Ph.D. Thesis, University of California at Davis, 1990.
35. E. L. Hjort, F. P. Brady, J. R. Drummond, B. McEachern, J. H. Osborne, J. L. Romero, D. S. Sorenson, and H. H. K. Tang, "65 MeV Fe, Sn, and Pb $(n, n'x)$ Measurements Over the Giant Resonance Continuum Region," Preprint, Department of Physics, University of California at Davis, 1994; submitted to *Phys. Rev. C.*
36. P. S. Rezentes, "Pre-Equilibrium Inclusive Spectra from Neutron-Induced Reactions with Silicon at Incident Energies of 50.0 and 32.2 MeV," Ph.D. Thesis, University of California at Davis, 1993.
37. P. S. Rezentes, C. M. Castaneda, J. L. Romero, H. H. K. Tang, T. A. Cahill, and J. D. Drummond, "Hydrogen and Helium Inclusive Spectra Produced by Neutron-Induced Reactions with Silicon at 50.0 and 32.2 MeV," Preprint, Department of Physics, University of California at Davis, 1995, to be published.
38. N. Azziz, H. H. K. Tang, and G. R. Srinivasan, "A Microscopic Model of Energy Deposition in Silicon Slabs Exposed to High-Energy Protons," *J. Appl. Phys.* **62**, 414–418 (1987).
39. H. Feshbach, A. K. Kerman, and S. E. Koonin, "The Statistical Theory of Multi-Step Compound and Direct Reactions," *Ann. Phys. (N.Y.)* **125**, 429–476 (1980).

40. E. Gadioli and P. E. Hodgson, *Pre-Equilibrium Nuclear Reactions, Oxford Studies in Nuclear Physics*, Vol. 15, Clarendon Press, Oxford, 1992.
41. R. L. Burman and E. S. Smith, "Parametrization of Pion Production and Reaction Cross Sections at LAMPF Energies," *Report No. LA-11502-MS, UC-414*, Los Alamos National Laboratory, Los Alamos, NM, May 1989.
42. R. L. Burman, M. E. Potter, and E. S. Smith, "Monte Carlo Simulation of Neutrino Production by Medium-Energy Protons in a Beam Stop," *Nucl. Instr. & Meth. A* **291**, 621–633 (1990).
43. D. Ashery, I. Navon, G. Azuelos, H. K. Walter, H. J. Pfeiffer, and F. W. Schleputz, "True Absorption and Scattering of Pions on Nuclei," *Phys. Rev. C* **23**, 2173 (1981).
44. A. Saunders, R. J. Peterson, R. A. Ristinen, S. Hoibraten, J. J. Kraushaar, B. J. Kriss, J. T. Brack, D. Ottewell, C. L. Morris, and E. F. Gibson, "Low Energy Pion–Nucleus Reaction and Total Cross Sections," Technical Progress Report, Nuclear Physics Laboratory and Department of Physics, University of Colorado, Boulder, 1994, pp. 42–45.
45. J. D. Zumbro, C. L. Morris, J. A. McGill, S. J. Seestrom, R. M. Whitton, C. M. Edwards, A. L. Williams, M. R. Braunstein, M. D. Kohler, B. J. Kriss, S. Hoibraten, R. J. Peterson, J. Ouyang, J. E. Wise, and W. R. Gibbs, "Inclusive Scattering of 500-MeV Pions from Carbon," *Phys. Rev. Lett.* **71**, 1796–1799 (1993).
46. J. E. Wise, M. R. Braunstein, S. Hoibraten, M. D. Kohler, B. J. Kriss, J. Ouyang, R. J. Peterson, J. A. McGill, C. L. Morris, S. J. Seestrom, R. M. Whitton, J. D. Zumbro, C. D. Edwards, and A. L. Williams, "Quasifree Pion Scattering at 500 MeV," *Phys. Rev. C* **48**, 1840–1848 (1993).
47. J. F. Dicello, M. Paciotti, and M. E. Schillaci, "An Estimate of Error Rates in Integrated Circuits at Aircraft Altitudes and at Sea Level," *Nucl. Instr. & Meth. B* **40/41**, 1295–1299 (1989).
48. J. F. Dicello, M. E. Schillaci, and L.-C. Liu, "Cross Sections for Pion, Proton, and Heavy-Ion Production from 800 MeV Protons Incident upon Aluminum and Silicon," *Nucl. Instr. & Meth. B* **45**, 135–138 (1990).
49. M. Blann, "Precompound Analyses of Spectra and Yields Following Nuclear Capture of Stopped π^-," *Phys. Rev. C* **28**, 1648–1662 (1983).
50. T. D. Lee, *Particle Physics and Introduction to Field Theory, Contemporary Concepts in Physics*, Vol. 1, Harwood Academic Publishers, New York, 1981.

Received July 15, 1994; accepted for publication February 24, 1995

Henry H. K. Tang *IBM Microelectronics Division, East Fishkill facility, Route 52, Hopewell Junction, New York 12533 (TANGH at FSHVMFK1, tangh@fshvmfk1.vnet.ibm.com).*
Dr. Tang received his B.A. degree (magna cum laude, with honors in physics and mathematics) from Kalamazoo College in 1974. He attended Yale University as an F. W. Heyl and Elsie L. Heyl Fellow and was awarded a Ph.D. degree in theoretical physics in 1979. His dissertation research was in the areas of nuclear many-body theory, nonequilibrium statistical mechanics of finite fermion systems and generalized mean-field theories, and hydrodynamic models of heavy ion reactions in the low- and intermediate-energy regimes. In 1979–80, Dr. Tang received a National Science Foundation Postdoctoral Fellowship in Nuclear Theory, and he was a visiting member of the Niels Bohr Institute at the University of Copenhagen. In 1980–82, he was appointed Research Associate in the Center for Theoretical Physics and Department of Physics at the Massachusetts Institute of Technology. In 1983, Dr. Tang joined the research staff of the Cyclotron Institute at Texas A&M University, where he was also on the visiting faculty of the Physics Department. In 1986, he joined IBM at East Fishkill, where he was engaged in modeling cosmic-ray-induced soft errors in microelectronic devices. For these efforts, he developed general nuclear reaction models. He is the author of the nuclear simulation codes, NUSPA, which generate databases for the soft-error simulators currently used throughout IBM. In the past few years, apart from radiation physics, Dr. Tang's work has also included high-field transport phenomena in submicron semiconductors and hydrodynamic modeling of advanced devices. He is currently involved in modeling NVRAM technologies. Dr. Tang is a member of the Phi Beta Kappa Society and the American Physical Society.